Applied Surface Science 396 (2017) 1783–1792

Contents lists available at ScienceDirect

Applied Surface Science

journal homepage: www.elsevier.com/locate/apsusc

Full Length Article

Performance of magnetic zirconium-iron oxide nanoparticle in the removal of phosphate from aqueous solution

Chang Zhang[a,b,*], Yongqiu Li[a,b], Fenghua Wang[c,**], Zhigang Yu[a,b], Jingjing Wei[a,b], Zhongzhu Yang[a,b], Chi Ma[a,b], Zihao Li[a,b], ZiYi Xu[a,b], Guangming Zeng[a,b]

[a] College of Environmental Science and Engineering, Hunan University, Changsha 410082, China
[b] Key Laboratory of Environmental Biology and Pollution Control (Hunan University), Ministry of Education, Changsha 410082, China
[c] Institute of Physical Education, Xinjiang Normal University, Urumqi 830054, China

ARTICLE INFO

Article history:
Received 2 September 2016
Received in revised form
16 November 2016
Accepted 27 November 2016
Available online 30 November 2016

Keywords:
Magnetic adsorbent
Molar ratios
Phosphate
Adsorption
Zirconium oxide

ABSTRACT

In this study, magnetic zirconium-iron oxide nanoparticles (MZION) of different Fe/Zr molar ratios were successfully prepared using the co-precipitation method, and their performance for phosphate removal was systematically evaluated. The as-obtained adsorbents were characterized by X-ray diffraction (XRD), scanning electron microscopy (SEM), transmission electron microscopy (TEM), Zeta potential analyzer, Fourier transform infrared spectroscopy (FT-IR) and Brunauer Emmett Teller (BET) specific surface area analysis. The effects of pH, ionic strength, and co-existing ions (including Cl^-, SO_4^{2-}, NO_3^- and HCO_3^-) were measured to evaluate the adsorption performance in batch experiments. The results showed that decreasing the Fe/Zr molar ratios increased the specific surface area that was propitious to adsorption process, but the adsorption capacity enhanced with the decrease of Fe/Zr molar ratios. Phosphate adsorption on MZION could be well described by the Freundlich equilibrium model and pseudo-second-order kinetics. The adsorption of phosphate was highly pH dependent and decreased with increasing pH from 1.5 to 10.0. The adsorption was slightly affected by ionic strength. With the exception of HCO_3^-, co-existing anions showed minimum or no effect on their adsorption performance. After adsorption, phosphate on these MZION could be easily desorbed by 0.1 M NaOH solution. The phosphate adsorption mechanism of MZION followed the inner-sphere complexing mechanism, and the surface —OH groups played a significant role in the phosphate adsorption. Additionally, the main advantages of MZION consisted in its separation convenience and highly adsorption capacity compared to other adsorbents.

1. Introduction

Phosphorus is an essential element that makes significant contribution to energy transport and biomass growth [1]. It is also an important material for agricultural and industrial products. However, an excessive intake of phosphorus in aquatic environment leads to an increase in cost associated with water treatment [2], accompanying significant eutrophication and water quality problems in rivers and lakes [3], and the growth of harmful algal blooms which may have an significantly influence on human health from the production of cyanotoxins [4]. Considering the serious health effects of phosphate, efficient techniques are urgently required to remove phosphate from wastewater.

Till now, several techniques, such as adsorption, chemical precipitation, ion exchange, biological process, membrane, reverse osmosis, and constructed wetland, have been developed to remove phosphate from wastewater [5–12]. Among these approaches, biological process is widely used in practical application [13], but it is quite sensitive to operation parameters including temperature [14], volatile fatty acid, cations, sludge quality and settlement, pH [15] and influent carbon source [16], resulting in decreased reliability and stability. Chemical precipitation is a costly process to remove phosphate, requiring the purchasing, transportation, and treatment of chemical precipitant, and producing a mass of sludge which needs further disposal [17]. Moreover, chemical precipitation is difficult to effectively remove phosphate at trace level [18]. Adsorption process is generally considered to be one of the most promising technologies because of its convenience, simplicity of design and operation, economics, and low-cost sorbents

* Corresponding author at: College of Environmental Science and Engineering, Hunan University, Changsha 410082, China.
** Corresponding author.
E-mail addresses: zhangchang@hnu.edu.cn (C. Zhang), 952157786@qq.com (F. Wang).

http://dx.doi.org/10.1016/j.apsusc.2016.11.214
0169-4332/

[19–22]. Comparatively, adsorption has significant advantages, especially low concentration phosphate, in removing phosphate from wastewater. Adsorbent is a key factor in the adsorption process. Over the past decades, a wide range of low-cost adsorbents have been examined for phosphate removal, including steel slag [23,24], surfactant modified zeolite [25,26], ferrihydrite [27,28], red mud [29,30], metal (hydro)oxides [31–33]. Although these adsorbents at nano-size have been demonstrated to be effective in phosphate adsorption because of their preferred surface properties and large surface areas [34,35], their large-scale application has been limited by the way of separation.

Magnetic separation was based on an external magnetic field to selectively collect the magnetic responsive materials. The addition of magnetic iron oxide was a conveniently separation method for removing phosphate from wastewater [36,37], but the main disadvantages of magnetic iron oxides adsorbent consisted in its disappointed adsorption capacity [38–40]. Fortunately, zirconium oxide has a strong affinity to phosphate and desorption for recycling [41], but it was suffering from the drawback of separation inconvenience [41,42]. Thus, zirconium oxide with magnetic property may be an attractive adsorbent choice for the removal phosphate from the contaminated water. Iron-zirconium oxides have been reported to be efficient for the removal of arsenic [43], antimony [44], hexavalent chromium [45] and phosphate [12]. Nevertheless, phosphate removal performance from aqueous solution using magnetic zirconium-iron oxide nanoparticle (MZION) both magnetic separation and with upper adsorption capacity has been rarely investigated to date.

In this essay, the phosphate removal performance of MZION was examined in details by both the equilibrium adsorption isotherm and kinetics study. The influences of various experimental conditions, such as ionic strength, co-existing anions and solution pH on phosphate removal were investigated. Desorption behavior and their reuse for phosphate adsorption were explored.

2. Material and methods

2.1. Chemicals

All chemicals were of analytical grade without further purification. Zirconium oxychloride octahydrate ($ZrOCl_2{\cdot}8H_2O$), ferric sulfate ($Fe_2(SO_4)_3$), ferrous sulfate ($FeSO_4{\cdot}7H_2O$), and sodium hydroxide (NaOH) were used as the raw material and purchased from Sinopharm Chemical Reagent Co., Ltd., Shanghai, P.R. China. Phosphate stock solution was prepared with deionized water using anhydrous potassium dihydrogen orthophosphate (KH_2PO_4, Sinopharm Chemical Reagent Co., Ltd., Shanghai, P.R. China).

2.2. Synthesis of MZION

MZION were synthesized with modification of the previous literature [38]. The adsorbents were prepared with different molar ratios of iron and zirconium, and the molar ratios of iron and zirconium were 2:1, 3:1, 6:1, 12:1, named S1, S2, S3, S4, respectively. Briefly, the solution of sodium hydroxide (NaOH, 6 M) was dropwisely added with vigorous mechanic stirring at room temperature into a 200 mL mixture solution of $FeSO_4{\cdot}7H_2O$ (0.25 M), $Fe_2(SO_4)_3$ (0.25 M) and $ZrOCl_2{\cdot}8H_2O$ to obtain a pH of 11. Subsequently, the resulting precipitates were aged at 90 °C for 18 h. After the reaction completed, the products were collected by magnet and then washed thoroughly with deionized water. The washed precipitates were then oven-dried at 90 °C for 8 h. Finally, the adsorbents were pulverized in a ball mill and kept at desiccator for further use.

2.3. Characterization analysis

The morphology of MZION was determined by scanning electron microscopy (FE-SEM S4800, Japan) and transmission electron microscopy (TEM, FEI Tecnai G20, USA). The X-ray diffraction (XRD) patterns of MZION were collected by Rigaku D/max-RB diffractometer with Cu-Kα radiation (λ = 0.15406 nm, 35 kV, 40 mA). Specific surface areas were evaluated by the nitrogen adsorption-desorption isotherms on a Quantachrome Instruments system via Brunauer- Emmett-Teller (BET) method. Pore size distribution was calculated by nitrogen desorption isotherm using Barret-Joymer-Halender (BJH) method. And the zeta potential of MZION suspension was determined by a Zeta Meter 3.0 (Zeta Meter Inc.). The FT-IR spectra of MZION before and after phosphate adsorption were measured on Fourier transformed infrared spectroscopy (FT-IR, Nicolet IS10). Magnetic property of MZION was analyzed by superconducting quantum interference devices magnetometer (SQUID, MPMS XL7, Quantum Desing, USA).

2.4. Batch sorption experiments

The batch adsorption experiments were conducted with 2.0 g L^{-1} MZION for phosphate solution in the 250 mL Erlenmeyer flasks at 293 ± 2 K, with 100 mL of initial phosphate concentrations ranging from 5 to 100 mg L^{-1}. The pH values were adjusted by addition of 0.1 M NaOH and 0.1 M HCl solution, and the contact time was 24 h. After equilibrium reached, the magnetic adsorbent was separated from the solution using a magnet and the phosphate concentrations were analyzed on a UV–vis spectrophotometer (SHIMADZU, UV-2550) at 880 nm according to the ammonium molybdate spectrophotometric method [8].

All the experiments were carried out in triplicate and the average value was used in this paper. The equilibrium adsorption capacity (Q_e, mg L^{-1}) and re-adsorption efficiency for phosphate were calculated by the following equation [46]:

$$Q_e = (C_o - C_e) \times \frac{\text{volume of the solution}}{\text{mass of adsorbent}}$$

$$\text{Removal efficiency} = \frac{(C_0 - C_e)}{C_0} \times 100\%$$

where Q_e is the amount of phosphate adsorbed on the magnetic adsorbent (mg g^{-1}), C_0 and C_e are the phosphate concentration in solution before and after adsorption (mg L^{-1}).

The adsorption kinetics was conducted with the initial phosphate concentration of 50 mg L^{-1} at pH = 4 ± 0.2 by allowing the reaction between the adsorbent and solution at various time intervals. Phosphate adsorption amount was calculated according to the following equation:

$$Q_t = (C_0 - C_t) \times \frac{\text{volume of the solution}}{\text{mass of adsorbent}}$$

where Q_t is the adsorpiton amount at time t (mg g^{-1}), C_0 is the initial concentration of phosphate solution (mg L^{-1}), C_t is the concentration of phosphate at time t (mg L^{-1}).

The effects of co-existing anions (Cl^-, SO_4^{2-}, NO_3^-, HCO_3^-) on phosphate adsorption were also investigated. The initial concentrations of co-existing anions were 0, 15, 30, 50, 100, 150 mg L^{-1}, respectively. The initial concentration of phosphate was fixed at 30 mg L^{-1}.

The regeneration and recyclability experiments of the MZION were performed by NaOH aqueous solution according to Su et al., [41]. NaOH aqueous solution was used as desorption solution. The initial phosphate concentration was 30 mg L^{-1} and the contact time was 24 h. After being separated by magnet, MZION were desorbed with NaOH solution. The desorbed nanoparticles were washed

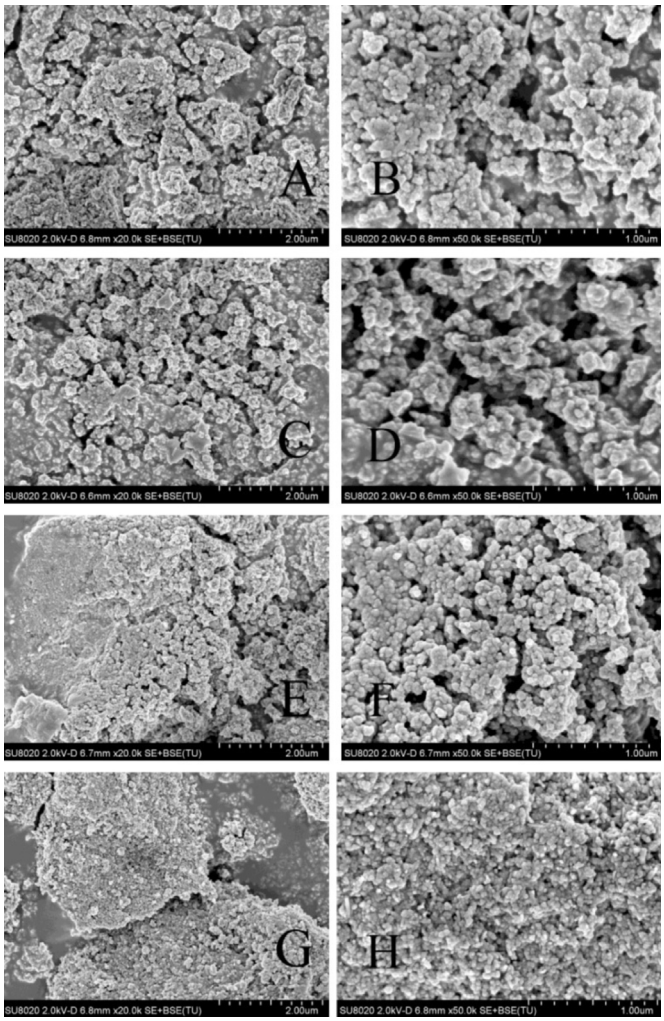

Fig. 1. SEM images of S1 (A, B), S2 (C, D), S3 (E, F), and S4 (G, H), respectively.

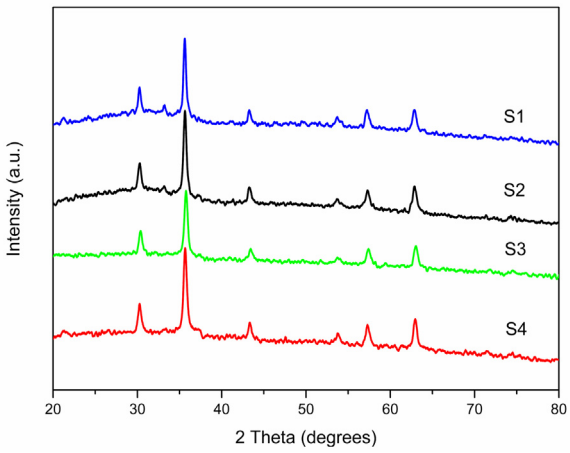

Fig. 2. XRD patterns of different molar ratios samples.

thoroughly with deionized water and dried at 90 °C for 8 h before they were used for phosphate adsorption again.

2.5. Effect of solution pH and ionic strength

The influence of pH of the initial solution and ionic strength on the uptake of phosphate was studied. The initial phosphate concentration was 40 mg L^{-1}, the solution pH was adjusted from 1.5 to 10.0, the concentrations of $NaNO_3$ were 0, 0.01, 0.1 M, respectively. 100 mL of phosphate solution was magnetic separately with 0.2 g of MZION in a series of 250 mL Erlenmeyer flasks at 293 K, and the contact time was 24 h.

3. Results and discussion

3.1. Characterization of MZION

As displayed in the SEM image (Fig. 1), the morphological characteristics of MZION were investigated in S1–S4, respectively. It can be clearly seen from Fig. 1 that the particles were agglomerated with nanoparticles, leading to a rough surface and a porous structure. The surface of particles became more and more rough with Fe/Zr molar ratios decreased, indicating that Fe/Zr molar ratios had an important effect on surface roughness.

XRD patterns of the original powders were shown in Fig. 2. These suggested that the samples were a clear amorphous structure and similar to the magnetic Fe-Zr binary oxide reported by Long et al., [36]. The XRD patterns of the synthesized materials were in good agreement with that of standard γ-Fe_2O_3 (maghemite, JCPDS card #39-1346) and Fe_3O_4 (magnetite, JCPDS card #65-3107). Peaks at 30.2°, 35.6°, 43.2° and 62.7° represented ZrO_2 (zirconium oxide, PDF#37-1413) were found. These results revealed that the principal components of magnetic adsorbents were zirconium oxide, maghemite and magnetite. Among them, the maghemite and magnetite were magnetic, which proved that the magnetic synthesized material was a composite of zirconium oxide and iron oxides.

TEM images in Fig. 3 directly demonstrated that MZION were quasi-spherical in shape with size of 10–50 nm, which was smaller than the magnetic Fe_3O_4@C@ZrO_2 (from 500 to700 nm) reported by Wang et al., [37] and had no obvious relationship with Fe/Zr molar ratios. From Fig. 3, each of the particles has a dark center surrounded by the pale skirt, suggesting the condensed inner magnetic cores and the less compact outer mesoporous shell [47], and the pale skirt scope enlarged with Fe/Zr molar ratios decreasing.

The relationships of pH versus surface zeta potential (ζ) for the magnetic absorbents were presented in Fig. 4. The point of zero charge (PZC) was significant in adsorption process because, given the anionic character of phosphate, surface charge of MZION can play an important role in terms of electrostatic interactions between the adsorbent and adsorbate. When the solution pH is below the PZC, the magnetic adsorbents will have a positive charge, promoting electrostatic attraction of the negatively charged phosphate ion. From Fig. 4, it was clearly showed that the zeta potential of all samples deceased with increasing pH due to the addition OH^-. Within different pH values ranging from 2 to 10, the PZC of S1–S4 were in the range of 8–9, which were higher than that of many other zirconium–iron binary oxides sorbent [12,36], and was in favor of the adsorption of phosphate from aqueous solution. The point of zero charge (PZC) of iron oxides was reported to around 6.1 [48], and higher PZC of MZION than that of iron oxides can be attributed to the deposition of ZrO_2 on MZION surface, which was in accordance with the results of previously reported [37,49].

The specific surface area and total pore volume of MZION were measured by nitrogen adsorption-desorption analysis, and the corresponding curves were shown in Fig. 5. The inset graph showed that the pore-size distribution of adsorbents (S1–S4) were in the range of 2–30 nm.

The data of specific surface area, average pore radius and pore volume of MIZON was listed in Table 1. According to the specific surface area analysis in Table 1, MIZON had larger surface area than other reported Zr-Fe binary oxides [44,45]. It can be seen that with an increase in Zr content, the specific surface area of MZION

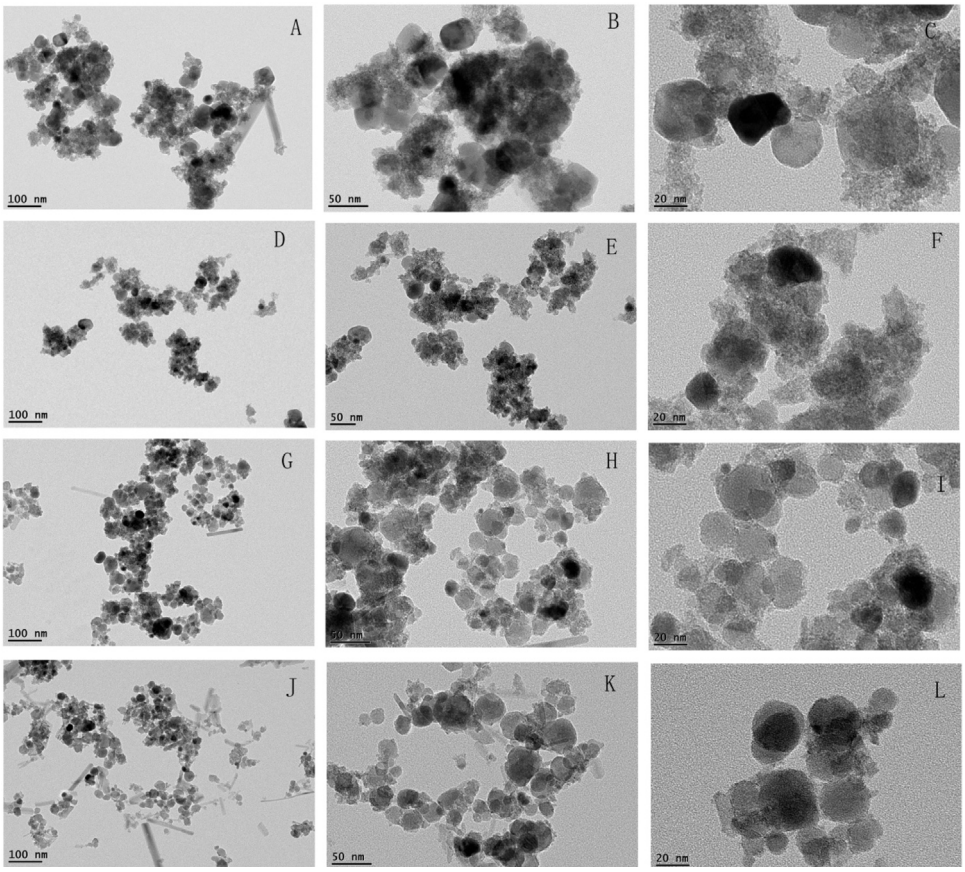

Fig. 3. TEM images of S1 (A–C), S2 (D–F), S3 (G–I) and S4 (J–L).

Table 1
Structure and pore properties of the magnetic adsorbents.

	S4	S3	S2	S1
Specific surface area (m^2/g)	124.36	150.34	213.50	282.02
Average pore radius (nm)	4.14	3.56	2.69	2.20
Pore volume (cm^3/g)	0.20	0.20	0.19	0.20

improved. On the contrary, the average pore radius decreased gradually and the pore volume almost didn't change with Zr content increasing. For S1, the specific surface area was as high as 282.02 m^2/g, while S3 was only 124.36 m^2/g. The increment of surface area might be ascribed to a decrease of average pore radius (from 4.14 to 2.20 nm), which was caused by the increase of Zr content in the magnetic adsorbents. with the Zr content increasing, the saturation magnetization of MZION decreased. It is suggested that lower saturation magnetization may have the effect to disperse iron oxides and zirconium oxides more uniformly, and resulted in significant enhancement of specific surface area. These results were consistent with SEM images, showing that the adsorbent morphology can be altered via the change of Fe/Zr molar ratio. Generally, sorbent with a smaller pore radius and larger pore volume possesses a superior surface area.

The Fourier-trans-formed infrared (FT-IR) spectra of S2 before and after phosphate adsorption were presented in Fig. 6. Before adsorption, the MZION was taken out from desiccator without further cleaning and was measured on Fourier transformed infrared spectroscopy. After adsorption, phosphate-loaded MZION was collected by magnet from aqueous solution, and then washed thoroughly with deionized water until the pH of washing water near to neutral. The washed precipitates were then oven-dried at 90 °C for 8 h. Finally, the phosphate-loaded MZION was measured on Fourier transformed infrared spectroscopy. The FT-IR data showed that the same major bands were found after and before adsorption. Without the phosphate adsorption, the FT-IR spectra of MZION had a strong bending (1638 cm^{-1}) vibrations of physically adsorbed H_2O and stretching (3363 cm^{-1}) vibration of hydroxyl groups [41], which indicated that MZION had a high adsorption ability to hydroxyl groups and H_2O existed on their surface. And the peak appearing at 1338 cm^{-1} was attributed to the deformation vibration of Zr-OH [42]. After phosphate adsorption, the FT-IR spectrum of MZION obviously changed. The peak of physically adsorbed H_2O and hydroxyl groups greatly narrowed, and the Zr-

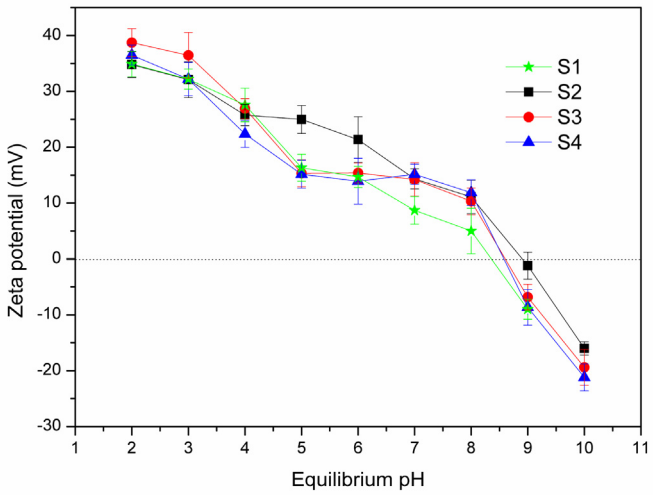

Fig. 4. Surface zeta potentials of S1–S4 as a function of pH.

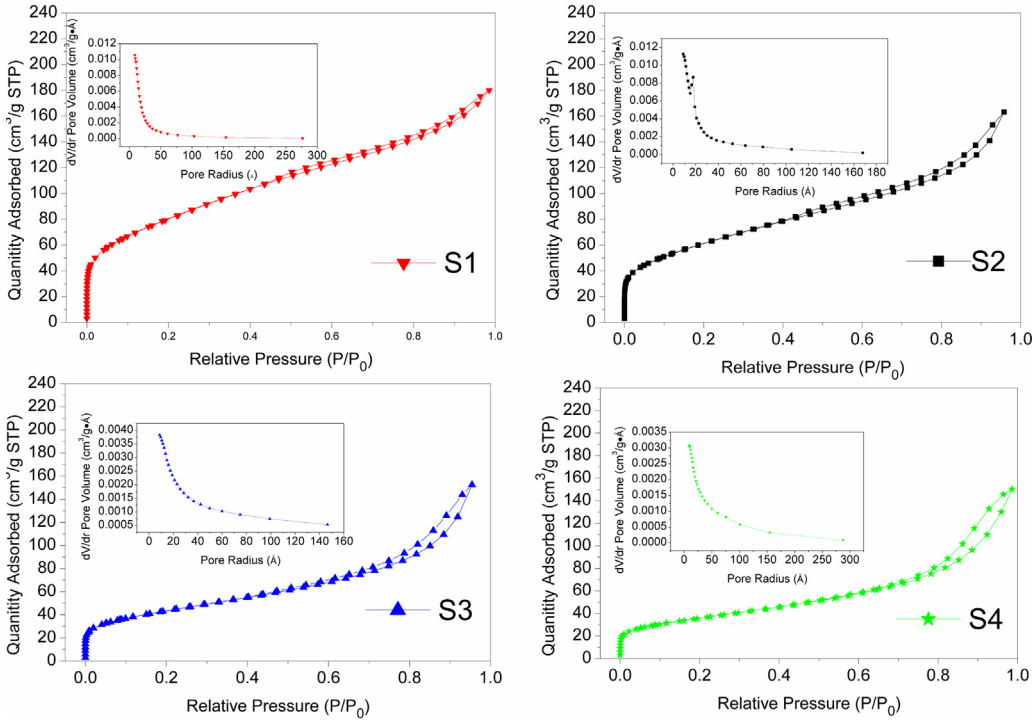

Fig. 5. N_2 adsorption-desorption isotherms of S1–S4. The inset is the corresponding pore-size distribution.

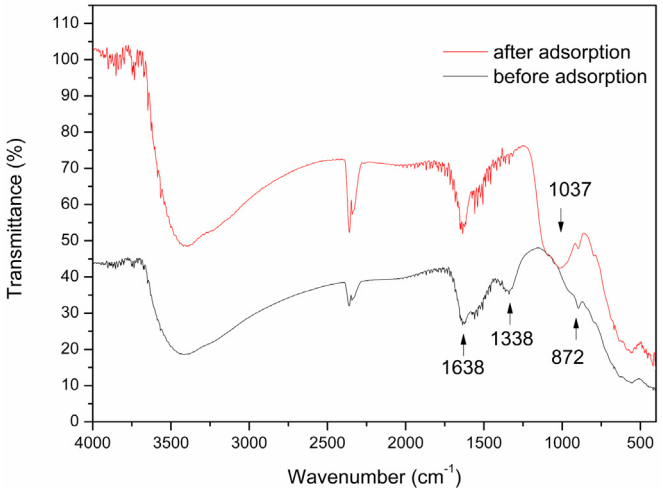

Fig. 6. FT-IR spectra of S2 after adsorption and before adsorption.

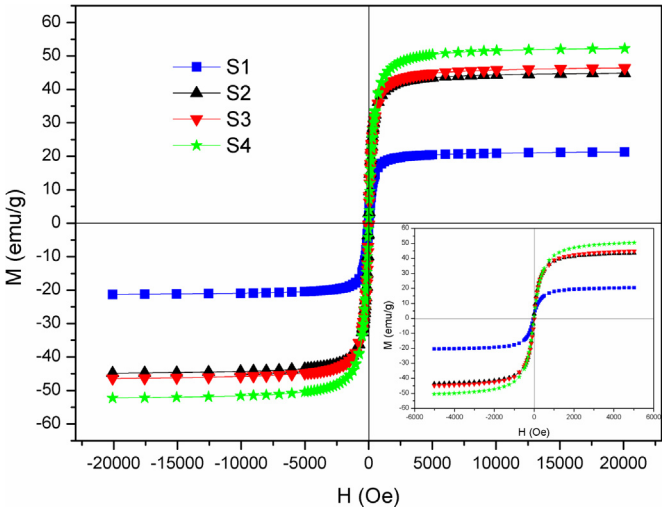

Fig. 7. Magnetization curves of S1–S4 at 300 K. Inset: the enlarged hyteresis loops with a scale ranging from −5000 to 5000 Oe.

OH deformation peak disappeared. These observations suggested that the replacement of physically adsorbed H_2O and hydroxyl groups occurred during the phosphate adsorption. Additionally, a broad and intensive peak appeared at 1037 cm^{-1}, which could be assigned to the asymmetry vibration of P—O bond, and suggested that the surface hydroxyl groups were replaced by the adsorbed phosphate [41]. The peak at 872 cm^{-1} was corresponded to the Fe—OH vibration [38]. The FT-IR results indicated that the Zr—OH groups played a key role in phosphate adsorption on MZION.

MPMS was used to determine the magnetic properties of different MZION at room temperature. Magnetic hysteresis curves of S1–S4 were shown in Fig. 7. All samples exhibited superparamagnetic because no magnetic hysteresis loops was observed. The saturation magnetization (Ms) values of as-obtained adsorbents were 21.3 emu/g for S1, 44.8 emu/g for S2, 45.4 emu/g for S3 and 52.2 emu/g for S4, respectively, indicating the higher Ms of S4 than that of S3, S2 and S1. With the Fe/Zr molar ratios increasing, the saturation magnetization of MZION increased. However, the saturation magnetization of all samples was sufficient for magnetic separation in the adsorption studies [50].

3.2. Equilibrium adsorption isotherms study

The equilibrium adsorption isotherms of phosphate onto MZION were evaluated by varying the initial phosphate concentrations. In this study, Freundlich isotherm model was used to estimate the adsorption capacity of MZION for phosphate. The equation of Freundlich model is represented as following Eq. (1) [51].

$$q_e = K_F C_e^{\frac{1}{n}} \quad (1)$$

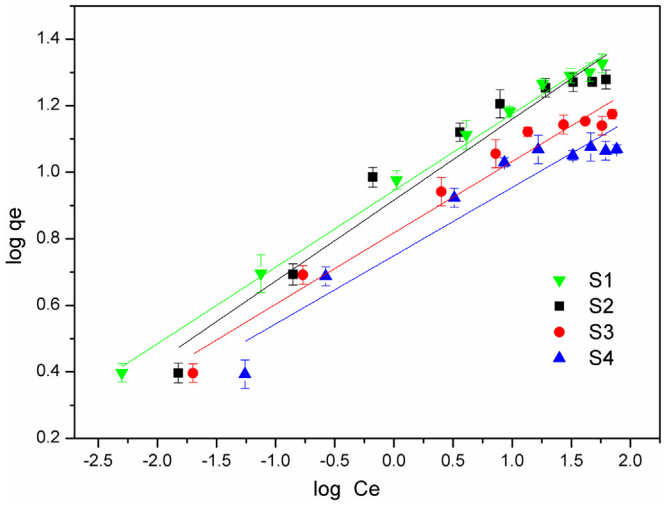

Fig. 8. Linearized Freundlich isotherm for phosphate adsorption by magnetic zirconium-iron oxide nanoparticle at 293 K.

Table 2
Freundlich isotherm parameters for adsorption of phosphate by magnetic adsorbents.

Adsorbents	K_F (mg g^{-1})	n	R^2
S1	2.59	4.34	0.9945
S2	2.51	4.11	0.9454
S3	2.28	4.66	0.9648
S4	2.16	4.87	0.9088

where q_e (mg g^{-1}) is the amount of phosphate adsorbed (equilibrium adsorption capacity) at equilibrium, C_e (mg L^{-1}) is the equilibrium concentration of phosphate in the aqueous solution, 1/n is the Freundlich constant related to the adsorption intensity and K_F is the Freundlich constant related to the adsorption capacity.

Phosphate adsorption on as-obtained zirconium-iron oxides fitted well with the Freundlich isotherm model (Fig. 8), suggesting a multilayer adsorption process. Table 2 summarized the Freundlich isotherm model parameters and their correlation coefficients. The equilibrium adsorption capacity of S1 for phosphate increased to 21.3 mg g^{-1} that slightly higher than 19.0 mg g^{-1}, 14.9 mg g^{-1} and 11.7 mg g^{-1} of S2–S4, respectively. And the sorption on the basis of per specific surface area of S1–S4 were 0.0755, 0.0889, 0.099 and 0.094 mg m^2, respectively. It was noticed that the content of zirconium of S1 was higher than S2–S4. Therefore, the adsorption of phosphate was mainly attributed to zirconium oxide, which was in agreement with the reported by Long et al. [36]. Moreover, MZION possessed a considerable adsorption capacity, compared to other magnetic adsorbents in literature, as shown in Table 3.

3.3. Adsorption kinetics

To understand the adsorption mechanism of phosphate on MZION, a kinetic investigation was conducted. Generally, an adsorption kinetic model provides valuable insights into the mechanism of sorption process [54]. In this study, kinetic data for phosphate adsorption onto MZION were fitted using different models.

Firstly, the pseudo-first-order kinetic equation and Ho's linearized pseudo-second-order [55] reaction rate models were conducted to describe the kinetic process. The mathematical forms of the two models are expressed as Eqs. (2) and (3), respectively.

$$\ln(q_e - q_t) = \ln q_e - k_1 t \quad (2)$$

$$\frac{t}{q_t} = \frac{1}{k_2 q_e^2} + \frac{1}{q_e} t \quad (3)$$

where q_e(mg g^{-1}) and q_t(mg g^{-1}) are the amount of phosphate adsorbed per unit mass of adsorbent at equilibrium and at any time t, k_1(min^{-1}) and k_2 (g mg^{-1} min^{-1}) are the equilibrium rate constants for pseudo-first-order and pseudo-second-order adsorption respectively, and t is the shaking time (min).

Results shown in Fig. 9a indicated that the amount of adsorbed phosphate increased with t and the adsorption process reached closely equilibrium state after 1000 min. The kinetic parameters data from pseudo-first-order model (Fig. 9b) and pseudo-second-order model (Fig. 9c) were listed in Table 4. The correlation coefficients (R^2) calculated from the pseudo-first-order kinetic model were 0.891–0.993, which were obviously lower than those of the correlation coefficient (R^2) obtained from pseudo-second-order kinetic model (0.995–0.999). Also, the experimental data of equilibrium adsorption capacity ($q_{e,exp}$ (mg g^{-1})) (S1 17.4, S2 16.9, S3 13.8, S4 10.4) were more closer to calculated data based on pseudo-second-order model (S1 17.6, S2 17.1, S3 14.0, S4 10.5) than pseudo-first-order model (S1 2.0, S2 2.3, S3 2.4, S4 2.1), respectively. The results from Table 4 suggested that the pseudo-first-order model was not applicable, which indicated that the mechanism of phosphate adsorption was chemisorption rather than physisorption for the pseudo-second-order model assuming a monolayer adsorption system.

As many reported literature put, intra-particle diffusion model was used to evaluate the rate-determining steps and mechanism in the adsorption process [56,57]. The rate q_t for intra-particle diffusion was expressed as Eq. (4) [8]:

$$q_t = k_p t^{1/2} + C \quad (4)$$

Table 3
Phosphate adsorption capacity of magnetic adsorbents reported in the literature.

Adsorbent	magnetite	Magnetic iron oxide	magnetite	Magnetic Fe_3O_4@C@ZrO_2	Magnetic Fe-Zr binary oxide	MZION
Adsorption capacity (mg P g^{-1})	3.2	5.03	5.2	13.99	13.65	21.3
Refs.	[39]	[38]	[52]	[53]	[36]	This study

Table 4
Kinetic parameters of phosphate adsorption to magnetic adsorbents based on the pseudo-first second order and pseudo-second order model.

Adsorbents	$q_{e,exp}{}^m$ (mg g^{-1})	Pseudo first- order			Pseudo second-order		
		K_1 (min^{-1})	$q_{e1}{}^n$ (mg g^{-1})	R^2	K_2 (g (mg^{-1} min^{-1}))	$q_{e2}{}^n$ (mg g^{-1})	R^2
S1	17.4	1.2×10^{-3}	2.0	0.891	2.431×10^{-3}	17.6	0.999
S2	16.9	9.6×10^{-4}	2.3	0.976	1.405×10^{-3}	17.1	0.998
S3	13.8	8.4×10^{-4}	2.4	0.993	9.52×10^{-4}	14.0	0.995
S4	10.4	8.0×10^{-4}	2.1	0.953	1.274×10^{-3}	10.5	0.996

Note: $q_{e,exp}{}^m$ is experimental values. $q_{e1}{}^n$, $q_{e2}{}^n$ are calculated values.

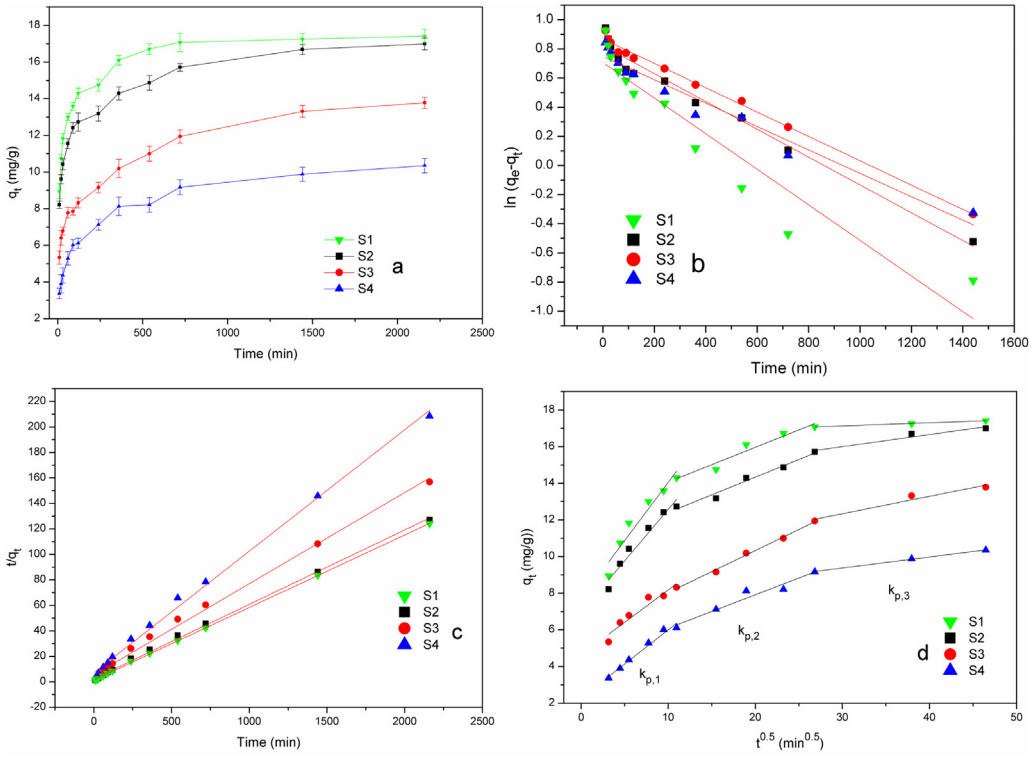

Fig. 9. (a) Adsorption kinetics of phosphate onto magnetic zirconium-iron oxide nanoparticle and (b) fitting with pseudo-first-order model; (c) pseudo-second-order model; (d) intra-particle diffusion model.

Table 5
Kinetic parameters of phosphate adsorption to magnetic adsorbents based on the intra-particle diffusion model.

Adsorbents	$K_{p,1}$ (mg (g^{-1} $min^{-0.5}$))	C (mg g^{-1})	R^2	$K_{p,2}$ (mg (g^{-1} $min^{-0.5}$))	C (mg g^{-1})	R^2	$K_{p,3}$ (mg (g^{-1} $min^{-0.5}$))	C (mg g^{-1})	R^2
S1	0.63	7.7	0.916	0.19	12.2	0.934	0.02	16.6	0.994
S2	0.56	7.0	0.945	0.19	10.4	0.971	0.06	14.0	0.904
S3	0.35	4.6	0.905	0.23	5.7	0.994	0.09	9.5	0.918
S4	0.37	2.3	0.975	0.18	4.2	0.934	0.05	7.6	0.998

where k_p (mg g^{-1} $min^{-0.5}$) is the intra-particle diffusion rate constant, q_t is the amount of phosphate adsorbed per unit mass of adsorbent (mg g^{-1}) at time t, and C is related to the thickness of the boundary layer. It can be seen from Fig. 9d that the plot of q_t versus $t^{0.5}$ for phosphate by MZION were multi-linear. The kinetic parameters of intra-particle diffusion of different magnetic adsorbents were listed in Table 5, which displayed that the adsorption rates were in the order of $k_{p,1} > k_{p,2} > k_{p,3}$ for all the sorbents and indicated that three or more steps occurred during the adsorption process. Firstly, the adsorption processes underwent a fast adsorption stage ($k_{p,1}$), and the subsequent plateau till equilibrium ($k_{p,2}$). Phosphate entered into the mesopore of adsorbents and was adsorbed by its interior surface after reaching saturation of exterior surface. As the decrease of the solute concentration, the adsorption process of phosphate finally reached the equilibrium stage ($k_{p,3}$).

The adsorption thermodynamics was performed at three different temperatures (293, 303 and 313 K). The thermodynamic parameters can be determined by the following equations [58]:

$$\Delta G^0 = \Delta H^0 - T\Delta S^0 \quad (5)$$

$$\Delta G^0 = -RT\ln K_d \quad (6)$$

$$\ln(K_d) = \frac{\Delta S^0}{R} - \frac{\Delta H^0}{RT}; \quad K_d = \frac{aq_e}{C_e} \quad (7)$$

where ΔS^0, ΔH^0, ΔG^0, R and T are entropy change (J mol^{-1}), enthalpy change (J mol^{-1}), Gibbs free energy (J mol^{-1}), universal gas constant (8.314 J (mol K) $^{-1}$), and temperature (K), respectively. K_d is the equilibrium constant, and a is the adsorbent dose (g L^{-1}). The values of ΔH^0 and ΔS^0were calculated by plotting ln(K_d) versus 1/T using Eq. (7) and the value of ΔG^0 was determined from Eq. (5).

Table 6
Thermodynamic parameters for phosphate adsorption onto magnetic adsorbents.

Adsorbents	Temp.(K)	ΔG(kJ mol^{-1})	ΔH(kJ mol^{-1})	ΔS(kJmol^{-1} K^{-1})
S1	293	−0.878	9.147	0.034
	303	−1.220		
	313	−1.563		
S2	293	−0.804	6.607	0.025
	303	−1.057		
	313	−1.310		
S3	293	−0.250	4.716	0.016
	303	−0.420		
	313	−0.589		
S4	293	0.357	3.940	0.012
	303	0.235		
	313	0.113		

The calculated thermodynamic parameters were presented in Table 6. The positive ΔH^0 and negative ΔG^0 for S1–S3 indicated the adsorption processes was endothermic and spontaneous. However, positive ΔG^0 had also been observed for phosphate adsorption onto S2, suggesting differences between the studied adsorption. The obtained positive ΔS^0 implied that the randomness increased

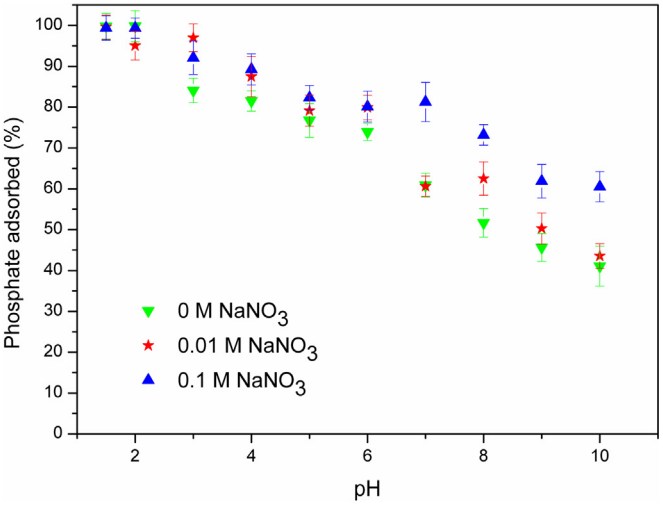

Fig. 10. Effect of pH and ionic strength on phosphate adsorption by S2.

at the interface between solution and solid during the adsorption process.

3.4. Influence of pH and ionic strength on phosphate adsorption

The effect of pH on phosphate adsorption to MZION was presented in Fig. 10. The results indicated that pH was a significant parameter on the process of adsorption. Increasing pH from 1.5 to 10 led to a monotonically decreased phosphate adsorption efficiency from 99.75% to 41.06%, which could be attributed to the competition between the phosphate ions and hydroxyl groups on the surface of the adsorbent [36]. The adsorption process based on the ion-exchange mechanism was reported as follows (Eqs. (8) and (9)) [59]:

$$Zr\text{-}OH + H_2PO_4^- = Zr(H_2PO_4) + OH^- \quad (8)$$

$$2Zr\text{-}OH + HPO_4^{2-} = Zr_2(H_2PO_4) + 2OH^- \quad (9)$$

Besides, the protonation of sorbent surface at high acidity was favorable for phosphate adsorption, as inferred from Eqs. (10)–(12):

$$Zr\text{-}OH + H^+ = Zr\text{-}OH_2^+ \quad (10)$$

$$Zr\text{-}OH_2^+ + H_2PO_4^- = (Zr\text{-}OH_2)^+(H_2PO_4)^- \quad (11)$$

$$2Zr\text{-}OH_2^+ + HPO_4^{2-} = (Zr\text{-}OH_2)_2^+(HPO_4)^{2-} \quad (12)$$

Hence, higher pH led to the deprotonation of adsorbent, invoking electrostatic repulsive interaction between anionic phosphate and negatively charged Zr—OH groups, and resulting in reduced phosphate adsorption.

The ionic strength effect on adsorption behavior can be used as an indicator for identifying the adsorption mechanism [60]. Fig. 10 showed that the phosphate sorption slightly enhanced with the increase of the solution ionic strength. It meant that MZION could be used as adsorbents to adsorb phosphate from high salinity wastewater. Consistently, similar observations for the phosphate adsorption on different adsorbents had been reported previously [12,59]. As reported by Su et al., [41], the adsorption of phosphate would either not change or increase with the increase of ionic strength if phosphate formed inner-sphere complexes, while the adsorption of phosphate would decrease with the increase of ionic strength if phosphate formed outer-sphere surface complexes. Therefore, the results in this study indicated that the adsorption of phosphate on MZION followed the inner-sphere complex mechanism.

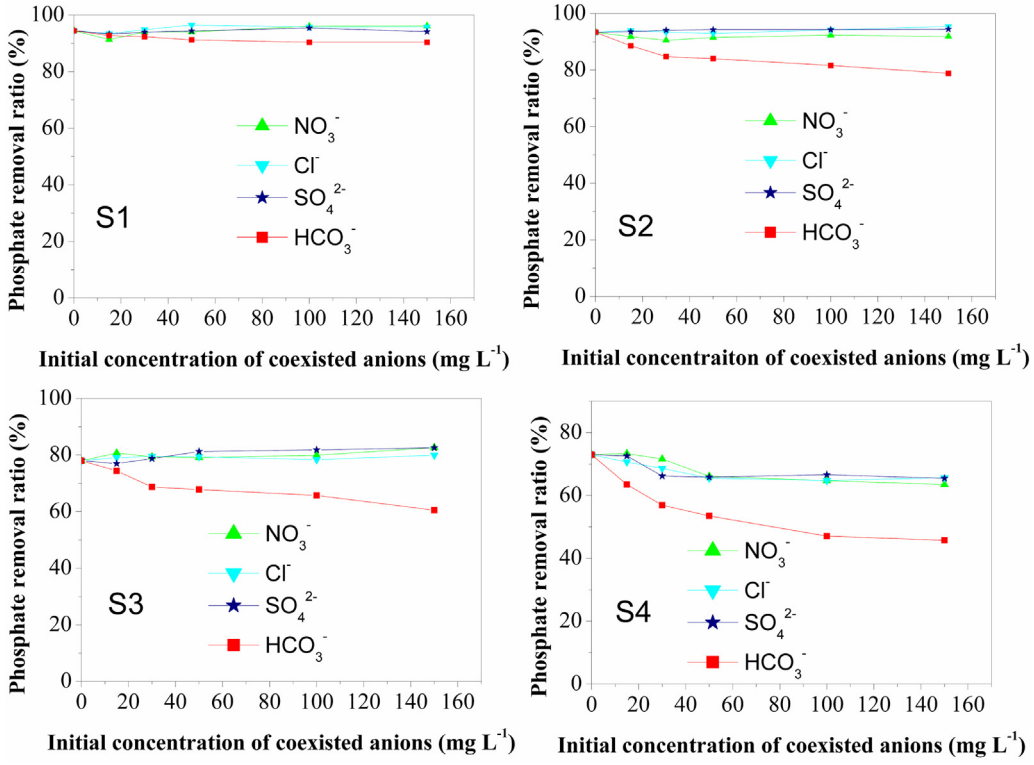

Fig. 11. Effect of co-existing anions on phosphate adsorption by magnetic zirconium-iron oxide nanoparticle.

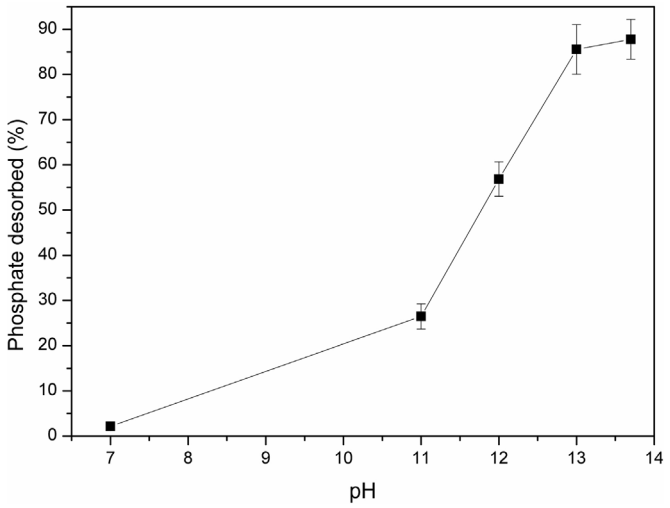

Fig. 12. Desorption of phosphate from phosphate-loaded S2 by NaOH solutions with different pH values.

3.5. Co-existing anion effect on phosphate adsorption by MZION

Adsorption selectivity was a significant factor influencing removal effectiveness. Highly selective adsorbents to remove or separate heavy metals from aqueous systems had been reported [61,62]. Wastewater always contains numerous aqueous constituents, which might compete for sorption sites and may largely affect the phosphate removal performance on adsorbents. Here, the effect of the commonly occurring anions (including Cl^-, SO_4^{2-}, NO_3^- and HCO_3^-) on phosphate removal by MZION was investigated, and the results were illustrated in Fig. 11.

For Cl^-, SO_4^{2-}, NO_3^-, no obvious decrease in phosphate removal ratio was observed when their concentrations increased from 0 to 150 mg L^{-1}. The results suggested that these three anions have no significant influence in the process of phosphate adsorption. However, the co-existing HCO_3^- restrained the phosphate adsorption. Taking S2 as an example, the phosphate removal ratio reduced from 93.38% to 78.83%, when the concentrations of HCO_3^- increased from 0 to 150 mg L^{-1}. This inhibition may be due to the strong competition for the adsorption sites on the adsorbent between the HCO_3^- and phosphate. Consequently, the uptake of phosphate gradually decreased as HCO_3^- concentration increased. In addition, with the increase of Fe/Zr molar ratios, the competitions between HCO_3^- and phosphate were more obvious. As illustrated above, the influence of HCO_3^- of phosphate removal on the MZION should be further investigated in the next study.

3.6. Desorption of phosphate from MZION and their reuse

Phosphate desorption tests were conducted using spent adsorbents to evaluate the possibility of adsorbent regeneration. Desorbability was defined as the ratio of phosphate desorbed over the total phosphate adsorbed by the adsorbents [8]. Thus, phosphate desorbability can manifest the degree of phosphate desorption from the adsorbents. The phosphate adsorbed on MZION could be desorbed with NaOH solution, and the results with NaOH solutions of different concentrations were showed in Fig. 12.

From Fig. 12, the phosphate desorbed percent ranged from 2.16% to 87.79%, with the concentration of NaOH solution increased from 0 M to 0.5 M. Results indicated that 0.1 M (pH13) NaOH solution could desorbed the preloaded phosphate on MZION with the efficiency higher than 85%. However, the further enhance of NaOH concentration to 0.5 M (pH 13.7) had not significantly effect on increasing the phosphate desorption. The spent MZION were reused for phosphate removal, which showed that they could maintain about 60%–70% of its original phosphate removal capability after re-adsorption for two cycles. Additionally, the adsorbent could be effectively separated by an external magnetic field. Thus, the recovered MZION could be reutilized for phosphate adsorption from wastewater, which may significantly cut down the operation cost.

4. Conclusions

MZION synthesized from a simple and low-cost co-precipitation process displayed an effective phosphate removal performance in aqueous solution in terms of both the adsorption capacity and separation convenience. The adsorption capacity on phosphate of S1 was determined at 21.3 mg g^{-1} at pH 4, which was higher than many reported magnetic adsorbents. As Fe/Zr molar ratios increase, the adsorption capacity decreased, and that of S2–S4 were 19.0, 14.9 and 11.7 mg g^{-1} at pH 4, respectively. The kinetic results showed that phosphate sorption onto MZION followed a pseudo-second-order kinetic model, suggesting its chemisorption. The adsorption mechanism of phosphate onto MZION was determined to follow the inner-sphere complexing mechanism, and the hydroxyl groups on the adsorbent surface played a major role in the phosphate removal. Its phosphate adsorption capacities decreased with decreasing pH. Higher point of zero charge makes the magnetic adsorbents also have remarkable adsorption ability, and the adsorbents maintained about 60%–70% of its original phosphate removal capability after two cycles. With the exception of HCO_3^-, commonly co-existing substances had little or no effect on phosphate removal. Thus, the needs for cost-feasible treatment for phosphate can be considered. The next studies should be addressed to investigate the competing mechanism between phosphate and HCO_3^- onto the MZION.

Acknowledgements

This work was supported by the National Natural Science Foundation of China (51521006). The authors are thankful to the anonymous reviewers for their enlightening comments and helpful suggestions to improve the paper.

References

[1] C.P. Slomp, P. Van Cappellen, The global marine phosphorus cycle: sensitivity to oceanic circulation, Biogeosciences 4 (2007) 155–171.
[2] W.K. Dodds, W.W. Bouska, J.L. Eitzmann, T.J. Pilger, K.L. Pitts, A.J. Riley, J.T. Schloesser, D.J. Thornbrugh, Eutrophication of U.S. freshwaters: analysis of potential economic damages, Environ. Sci. Technol. 43 (2009) 12–19.
[3] D.J. Conley, H.W. Paerl, R.W. Howarth, D.F. Boesch, S.P. Seitzinger, K.E. Havens, C. Lancelot, G.E. Likens, ECOLOGY controlling eutrophication: nitrogen and phosphorus, Science 323 (2009) 1014–1015.
[4] D. Anderson, P. Glibert, J. Burkholder, Harmful algal blooms and eutrophication: nutrient sources, composition, and consequences, Estuaries 25 (2002) 704–726.
[5] E.M. van Voorthuizen, A. Zwijnenburg, M. Wessling, Nutrient removal by NF and RO membranes in a decentralized sanitation system, Water Res. 39 (2005) 3657–3667.
[6] X. Zheng, J. Pan, F. Zhang, E. Liu, W. Shi, Y. Yan, Fabrication of free-standing bio-template mesoporous hybrid film for high and selective phosphate removal, Chem. Eng. J. 284 (2016) 879–887.
[7] G.-x. He, L.-h. He, Z.-w. Zhao, X.-y. Chen, L.-l. Gao, X.-h. Liu, Thermodynamic study on phosphorus removal from tungstate solution via magnesium salt precipitation method, Trans. Nonferr. Metal Soc. 23 (2013) 3440–3447.
[8] J. Lalley, C. Han, X. Li, D.D. Dionysiou, M.N. Nadagouda, Phosphate adsorption using modified iron oxide-based sorbents in lake water: kinetics, equilibrium, and column tests, Chem. Eng. J. 284 (2016) 1386–1396.
[9] L.E. de-Bashan, Y. Bashan, Recent advances in removing phosphorus from wastewater and its future use as fertilizer (1997–2003), Water Res. 38 (2004) 4222–4246.
[10] L.M. Blaney, S. Cinar, A.K. SenGupta, Hybrid anion exchanger for trace phosphate removal from water and wastewater, Water Res. 41 (2007) 1603–1613.

[11] L. Song, J. Huo, X. Wang, F. Yang, J. He, C. Li, Phosphate adsorption by a Cu(II)-loaded polyethersulfone-type metal affinity membrane with the presence of coexistent ions, Chem. Eng. J. 284 (2016) 182–193.
[12] Z. Ren, L. Shao, G. Zhang, Adsorption of phosphate from aqueous solution using an iron–zirconium binary oxide sorbent, Water Air Soil Pollut. 223 (2012) 4221–4231.
[13] S.Y. Gebremariam, M.W. Beutel, D. Christian, T.F. Hess, Research advances and challenges in the microbiology of enhanced biological phosphorus removal—a critical review, Water Environ. Res. 83 (2011) 195–219.
[14] T. Panswad, A. Doungchai, J. Anotai, Temperature effect on microbial community of enhanced biological phosphorus removal system, Water Res. 37 (2003) 409–415.
[15] D. Mulkerrins, A.D.W. Dobson, E. Colleran, Parameters affecting biological phosphate removal from wastewaters, Environ. Int. 30 (2004) 249–259.
[16] A. Oehmen, R.J. Zeng, J. Keller, Z. Yuan, Modeling the aerobic metabolism of polyphosphate-accumulating organisms enriched with propionate as a carbon source, Water Environ. Res. 79 (2007) 2477–2486.
[17] D.W. de Haas, M.C. Wentzel, G.A. Ekama, The use of simultaneous chemical precipitation in modified activated sludge systems exhibiting biological excess phosphate removal part 1: literature review, Water S.A. 26 (2000) 439–452.
[18] M.R. Awual, A. Jyo, T. Ihara, N. Seko, M. Tamada, K.T. Lim, Enhanced trace phosphate removal from water by zirconium(IV) loaded fibrous adsorbent, Water Res. 45 (2011) 4592–4600.
[19] A. Bhatnagar, M. Sillanpää, A review of emerging adsorbents for nitrate removal from water, Chem. Eng. J. 168 (2011) 493–504.
[20] A. Zach-Maor, R. Semiat, H. Shemer, Synthesis, performance, and modeling of immobilized nano-sized magnetite layer for phosphate removal, J. Colloid Interface Sci. 357 (2011) 440–446.
[21] L. Zeng, X. Li, J. Liu, Adsorptive removal of phosphate from aqueous solutions using iron oxide tailings, Water Res. 38 (2004) 1318–1326.
[22] F. Ni, J. He, Y. Wang, Z. Luan, Preparation and characterization of a cost-effective red mud/polyaluminum chloride composite coagulant for enhanced phosphate removal from aqueous solutions, J. Water Process Eng. 6 (2015) 158–165.
[23] C. Barca, C. Gérente, D. Meyer, F. Chazarenc, Y. Andrès, Phosphate removal from synthetic and real wastewater using steel slags produced in Europe, Water Res. 46 (2012) 2376–2384.
[24] L.I. Bowden, A.P. Jarvis, P.L. Younger, K.L. Johnson, Phosphorus removal from waste waters using basic oxygen steel slag, Environ. Sci. Technol. 43 (2009) 2476–2481.
[25] A. Naghash, A. Nezamzadeh-Ejhieh, Comparison of the efficiency of modified clinoptilolite with HDTMA and HDP surfactants for the removal of phosphate in aqueous solutions, J. Ind. Eng. Chem. 31 (2015) 185–191.
[26] J. Schick, P. Caullet, J.-L. Paillaud, J. Patarin, S. Freitag, C. Mangold-Callarec, Phosphate uptake from water on a surfactant-modified zeolite and Ca-zeolites, J. Porous Mater. 19 (2012) 405–414.
[27] J. Antelo, F. Arce, S. Fiol, Arsenate and phosphate adsorption on ferrihydrite nanoparticles. Synergetic interaction with calcium ions, Chem. Geol. 410 (2015) 53–62.
[28] H. Wang, J. Zhu, Q.-L. Fu, J.-W. Xiong, C. Hong, H.-Q. Hu, A. Violante, Adsorption of phosphate onto ferrihydrite and ferrihydrite-Humic acid complexes, Pedosphere 25 (2015) 405–414.
[29] W. Huang, S. Wang, Z. Zhu, L. Li, X. Yao, V. Rudolph, F. Haghseresht, Phosphate removal from wastewater using red mud, J. Hazard. Mater. 158 (2008) 35–42.
[30] Y. Zhao, Q. Yue, Q. Li, X. Xu, Z. Yang, X. Wang, B. Gao, H. Yu, Characterization of red mud granular adsorbent (RMGA) and its performance on phosphate removal from aqueous solution, Chem. Eng. J. 193–194 (2012) 161–168.
[31] J. Majzlan, Thermodynamic stabilization of hydrous ferric oxide by adsorption of phosphate and arsenate, Environ. Sci. Technol. 45 (2011) 4726–4732.
[32] I. de Vicente, P. Huang, F.Ø. Andersen, H.S. Jensen, Phosphate adsorption by fresh and aged aluminum hydroxide. Consequences for lake restoration, Environ. Sci. Technol. 42 (2008) 6650–6655.
[33] B. Pan, F. Han, G. Nie, B. Wu, K. He, L. Lu, New strategy to enhance phosphate removal from water by hydrous manganese oxide, Environ. Sci. Technol. 48 (2014) 5101–5107.
[34] Y. Su, W. Yang, W. Sun, Q. Li, J.K. Shang, Synthesis of mesoporous cerium–zirconium binary oxide nanoadsorbents by a solvothermal process and their effective adsorption of phosphate from water, Chem. Eng. J. 268 (2015) 270–279.
[35] J. Lǔ, H. Liu, R. Liu, X. Zhao, L. Sun, J. Qu, Adsorptive removal of phosphate by a nanostructured Fe–Al–Mn trimetal oxide adsorbent, Powder Technol. 233 (2013) 146–154.
[36] F. Long, J.-L. Gong, G.-M. Zeng, L. Chen, X.-Y. Wang, J.-H. Deng, Q.-Y. Niu, H.-Y. Zhang, X.-R. Zhang, Removal of phosphate from aqueous solution by magnetic Fe–Zr binary oxide, Chem. Eng. J. 171 (2011) 448–455.
[37] W. Wang, H. Zhang, L. Zhang, H. Wan, S. Zheng, Z. Xu, Adsorptive removal of phosphate by magnetic Fe3O4@C@ZrO2, Colloid Surf. A 469 (2015) 100–106.
[38] S.-Y. Yoon, C.-G. Lee, J.-A. Park, J.-H. Kim, S.-B. Kim, S.-H. Lee, J.-W. Choi, Kinetic, equilibrium and thermodynamic studies for phosphate adsorption to magnetic iron oxide nanoparticles, Chem. Eng. J. 236 (2014) 341–347.
[39] G. Pan, L. Li, D. Zhao, H. Chen, Immobilization of non-point phosphorus using stabilized magnetite nanoparticles with enhanced transportability and reactivity in soils, Environ. Pollut. 158 (2010) 35–40.
[40] T.J. Daou, S. Begin-Colin, J.M. Grenèche, F. Thomas, A. Derory, P. Bernhardt, P. Legaré, G. Pourroy, Phosphate adsorption properties of magnetite-based nanoparticles, Chem. Mater. 19 (2007) 4494–4505.
[41] Y. Su, H. Cui, Q. Li, S. Gao, J.K. Shang, Strong adsorption of phosphate by amorphous zirconium oxide nanoparticles, Water Res. 47 (2013) 5018–5026.
[42] H. Cui, Q. Li, S. Gao, J.K. Shang, Strong adsorption of arsenic species by amorphous zirconium oxide nanoparticles, J. Ind. Eng. Chem. 18 (2012) 1418–1427.
[43] Z. Ren, G. Zhang, J. Paul Chen, Adsorptive removal of arsenic from water by an iron–zirconium binary oxide adsorbent, J. Colloid Interface Sci. 358 (2011) 230–237.
[44] X. Li, X. Dou, J. Li, Antimony(V) removal from water by iron-zirconium bimetal oxide: performance and mechanism, J. Environ. Sci. 24 (2012) 1197–1203.
[45] Y. Wang, D. Liu, J. Lu, J. Huang, Enhanced adsorption of hexavalent chromium from aqueous solutions on facilely synthesized mesoporous iron–zirconium bimetal oxide, Colloid Surf. A 481 (2015) 133–142.
[46] C. Zhang, Z. Yu, G. Zeng, B. Huang, H. Dong, J. Huang, Z. Yang, J. Wei, L. Hu, Q. Zhang, Phase transformation of crystalline iron oxides and their adsorption abilities for Pb and Cd, Chem. Eng. J. 284 (2016) 247–259.
[47] G. Li, Z. Zhao, J. Liu, G. Jiang, Effective heavy metal removal from aqueous systems by thiol functionalized magnetic mesoporous silica, J. Hazard. Mater. 192 (2011) 277–283.
[48] G. Zhang, H. Liu, R. Liu, J. Qu, Removal of phosphate from water by a Fe–Mn binary oxide adsorbent, J. Colloid Interface Sci. 335 (2009) 168–174.
[49] W. Wang, J. Zhou, D. Wei, H. Wan, S. Zheng, Z. Xu, D. Zhu, ZrO2-functionalized magnetic mesoporous SiO2 as effective phosphate adsorbent, J. Colloid Interface Sci. 407 (2013) 442–449.
[50] N. Wang, L. Zhou, J. Guo, Q. Ye, J.-M. Lin, J. Yuan, Adsorption of environmental pollutants using magnetic hybrid nanoparticles modified with β-cyclodextrin, Appl. Surf. Sci. 305 (2014) 267–273.
[51] N. Rahman, U. Haseen, Equilibrium modeling, kinetic, and thermodynamic studies on adsorption of Pb (II) by a hybrid inorganic–organic material: polyacrylamide zirconium (IV) iodate, Ind. Eng. Chem. Res. 53 (2014) 8198–8207.
[52] T. Daou, S. Begin-Colin, J. Greneche, F. Thomas, A. Derory, P. Bernhardt, P. Legaré, G. Pourroy, Phosphate adsorption properties of magnetite-based nanoparticles, Chem. Mater. 19 (2007) 4494–4505.
[53] W. Wang, H. Zhang, L. Zhang, H. Wan, S. Zheng, Z. Xu, Adsorptive removal of phosphate by magnetic Fe 3 O 4@ C@ ZrO 2, Colloid Surf. A 469 (2015) 100–106.
[54] Y.S. Ho, G. McKay, Pseudo-second order model for sorption processes, Process. Biochem. 34 (1999) 451–465.
[55] T. Wang, X. Xu, Z. Ren, B. Gao, H. Wang, Adsorption of phosphate on surface of magnetic reed: characteristics, kinetic, isotherm, desorption, competitive and mechanistic studies, RSC Adv. 6 (2016) 5089–5099.
[56] G. Zeng, Y. Liu, L. Tang, G. Yang, Y. Pang, Y. Zhang, Y. Zhou, Z. Li, M. Li, M. Lai, X. He, Y. He, Enhancement of Cd(II) adsorption by polyacrylic acid modified magnetic mesoporous carbon, Chem. Eng. J. 259 (2015) 153–160.
[57] Q. Sun, L. Yang, The adsorption of basic dyes from aqueous solution on modified peat–resin particle, Water Res. 37 (2003) 1535–1544.
[58] A. Goswami, M.K. Purkait, Kinetic and equilibrium study for the fluoride adsorption using pyrophyllite, Sep. Sci. Technol. 46 (2011) 1797–1807.
[59] H. Liu, X. Sun, C. Yin, C. Hu, Removal of phosphate by mesoporous ZrO 2, J. Hazard. Mater. 151 (2008) 616–622.
[60] S. Goldberg, C.T. Johnston, Mechanisms of arsenic adsorption on amorphous oxides evaluated using macroscopic measurements, vibrational spectroscopy, and surface complexation modeling, J. Colloid Interface Sci. 234 (2001) 204–216.
[61] X. Chen, K.F. Lam, K.L. Yeung, Selective removal of chromium from different aqueous systems using magnetic MCM-41 nanosorbents, Chem. Eng. J. 172 (2011) 728–734.
[62] K.F. Lam, X. Chen, C.M. Fong, K.L. Yeung, Selective mesoporous adsorbents for Ag+/Cu2+ separation, Chem. Commun. (2008) 2034–2036.